Max-Planck-Institut für Meteorologie

REPORT No. 153

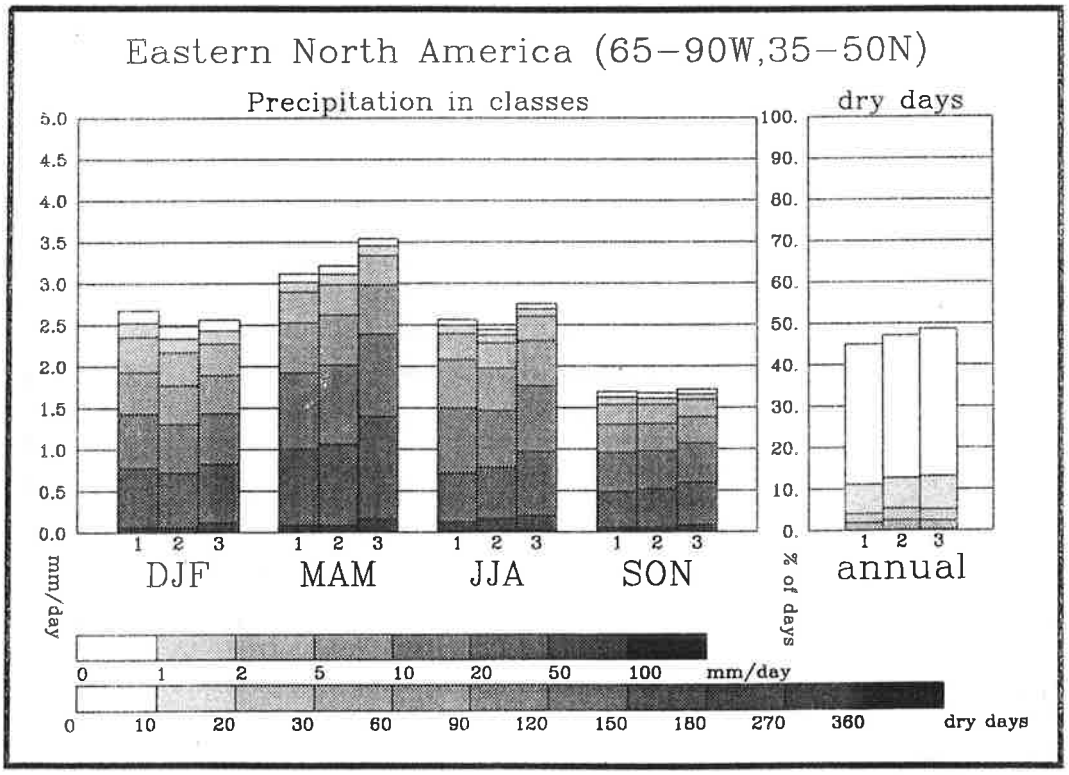

REGIONAL CLIMATE CHANGES AS SIMULATED IN TIME-SLICE EXPERIMENTS

by

ULRICH CUBASCH · JÜRGEN WASZKEWITZ
GABI C. HEGERL · JAN PERLWITZ

HAMBURG, February 1995

AUTHORS:

Ulrich Cubasch
Jürgen Waszkewitz
Jan Perlwitz

Deutsches Klima Rechenzentrum GmbH
Bundesstr. 55
D-20146 Hamburg
Germany

Gabi C. Hegerl

Max-Planck-Institut
für Meteorologie

MAX-PLANCK-INSTITUT
FÜR METEOROLOGIE
BUNDESSTRASSE 55
D-20146 Hamburg
F.R. GERMANY

Tel.: +49-(0)40-4 11 73-0
Telefax: +49-(0)40-4 11 73-298
E-Mail: <name> @ dkrz.d400.de

REPb 153

Regional climate changes as simulated in time-slice experiments

U. Cubasch[1], J. Waszkewitz[1], G. Hegerl[2] and J. Perlwitz[1]

1: Deutsches Klimarechenzentrum GmbH, Bundesstr. 55, 20146 Hamburg, Germany

2: Max-Planck-Institut für Meteorologie, Bundesstr. 55, 20146 Hamburg, Germany

ISSN 0937-1060

Abstract

Three 30 year long simulations have been performed with a T42 atmosphere model, in which the sea-surface temperature (SST) and sea-ice distribution has been taken from a transient climate change experiment with a T21 global coupled ocean-atmosphere model. In this so-called time-slice experiment, the SST values (and the greenhouse gas concentration) were taken at present time CO_2 level, at the time of CO_2 doubling and tripling.

The annual cycle of temperature and precipitation has been studied over the IPCC regions and has been compared with observations. Additionally the combination of temperature and precipitation change has been analysed. Further parameters investigated include the difference between daily minimum and maximum temperature, the rainfall intensity and the length of droughts.

While the regional simulation of the annual cycle of the near surface temperature is quite realistic with deviations rarely exceeding 3K, the precipitation is repoduced to a much smaller degree of accuracy.

The temperature changes nonlinearly in response to the enhanced greenhouse forcing. This is connected with the cold start of the transient simulation. The changes in temperature at the time of CO_2 doubling amount to only 30%-40% of those at the $3*CO_2$ level and show hardly any seasonal variation, contrary to the $3*CO_2$ experiment. Due to the delay in warming, the $3*CO_2$ experiment can be compared to the CO_2 doubling studies performed with mixed-layer models. The precipitation change does not display a clear signal. However, an increase of the rain intensity and of longer dry periods is simulated in many regions of the globe.

The changes in these parameters as well as the combination of temperature- and precipitation change and the changes in the daily temperature range give valuable hints, in which regions observational studies should be intensified and under which aspects the observational data should be evaluated.

1.0 Introduction

Even though global warming has been much in debate during the last decade, there is still a difference in the quantities the modelers analyse (mainly those they know they can trust most in their models) and those, which effect the daily life. The perception of the public suggest that the climate change has an visible impact on a number of meteorological parameters like temperature, storms, droughts, precipitation and so on. However, this perception can rarely be verified with observational data, since only few data exist in a coherent form and only for a limited number of regions.

Studies to verify possible connections between climate change as predicted by the models and regional observations have been carried out in a number of studies. However, these studies have attracted a lot of criticisms, since it was felt that the model resolution was too coarse and the model performance was too poor to allow for a regional interpretation of the results (v. Storch et al, 1993; Grotch and McCracken, 1991, Wigley et al, 1990). Various techniques are currently been employed to overcome this problem. Besides statistical methods (v. Storch et al, 1993), dynamical regional high resolution models have been nested into global models (for an overview see: Giorgi and Mearns, 1991). These regional models have the advantage that affordable very high resolution time-slice simulations can be performed for a certain region of interest, but have the disadvantage that they encounter severe problems at the boundaries and that they are currently coupled only one way, i. e. an interaction of the regional scale with the global scale is not possible. An alternative strategy using dynamical models is the so called „time slice" method using a global atmosphere model.

The present study investigates regional changes with a higher resolution global general circulation model (on a Gaussian grid of ca. 2.8^0) using the time-slice method. In this technique an atmosphere model is forced by the changed greenhouse gas concentration, while the sea surface temperature (SST) and sea ice distribution is taken from a transient simulation with a coarse resolution (Gaussian grid of 5.6^0, see Cubasch et al, 1992) globally coupled ocean-atmosphere model (Perlwitz et al, 1994; Mahfouf et al,

1994). This method has the advantage that the model can be integrated for several decades around the time of interest with a high resolution, and that it gives a large statistical sample of the changed climate similar to equilibrium experiments with mixed-layer models (IPCC, 1990). Additionally it has a more credible distribution of the SST than the mixed layer models.

Currently there is a growing interest to identify variables suitable for the detection of the climate change. These variables should have a high signal to noise ratio (Santer et al, 1993), and should also be easy to measure and should have been recorded in the past. As longer records only exist on a regional scale, it is of particular interest to identify not only the parameters but also the regions which are optimal for the detection.

At first it will be analysed how well the model simulates the seasonal cycle of basic weather parameters and whether the seasonal cycle is changed (section 3.1) under the increased greenhouse gas concentration (section 3.1). The analysis will focus on the near surface temperature (section 3.1.1) and the precipitation (section 3.1.2). A number of studies have dealt with the question how the climate change will impact the plant growth and how vegetation regions are shifted (Lohmann et al, 1993; Claussen and Esch, 1992). While these vegetation models mainly use a combination of precipitation and temperature, a shift in vegetation is a quantity difficult to observe. Some observational studies suggest that the combination of precipitation- and temperature change is a better indicator for the climate change than either variable on its own (Karl, 1995, pers. com.). Such a combination is analysed in section 3.1.3.

Studies in North America suggest that the observed global warming is in some regions partially due to a larger rise in the minimum temperature than in the maximum temperature (Karl et al, 1994). In section 3.2 we will investigate whether this effect can be found in climate models as well, and whether it can be found globally or only in specific regions.

Observational findings from North America (Karl et al, 1995) indicate that there is a tendency of an increase of the "strong" rainfall. This supposition will be tested with the model results as well (section 3.3).

Finally, after the severe drought in Central US in the year 1988 it has been stated by some scientist that this is a clear indicator of the greenhouse effect. The model results are used to estimate the length of drought periods in a changed climate (section 3.5).

2.0 The model and the experiment

The model employed is the T42 version of the ECHAM3 model (DKRZ, 1992). It is a spectral transform model with a triangular truncation and has a vertical resolution of 19 levels. The parametrization of sub-grid scale processes, which is performed on a Gaussian grid of ca. 2.8^0, includes a radiation scheme with a broad-band formulation of the radiative transfer equation with six spectral intervals in the infrared and four intervals in the solar part of the spectrum (Hense et al, 1982; Rockel et al, 1991). Gaseous absorption due to water vapor, carbon dioxide and ozone is taken into account as well as scattering and absorption due to aerosols and clouds. The cloud optical properties are parameterized in terms of cloud water content which is an explicit variable of the model.

The vertical turbulent transfer of momentum, heat, water vapor and cloud water is based upon the Monin-Obukov similarity theory for the surface layer and the eddy diffusivity approach above the surface layer (Louis, 1979). The drag and heat transfer coefficients depend on roughness length and Richardson number, and the eddy diffusion coefficients depend on wind stress, mixing length and Richardson number, which has been reformulated in terms of cloud-conservative variables (Brinkop, 1992).

The effect of orographically excited gravity waves on the momentum budget is parameterized on the basis of linear theory and dimensional considerations (Miller et al, 1989). The vertical structure of the momentum flux induced by the gravity waves is

calculated from a local Richardson number which describes the onset of turbulence due to convective instability.

The parametrization of cumulus convection is based on the concept of mass flux and comprises the effect of deep, shallow and mid-level convection on the budget of heat, water vapor and momentum (Tiedtke, 1989). Cumulus clouds are represented by a bulk model including the effect of entrainment and detrainment on the updraft and downdraft convective mass fluxes. Mixing due to shallow stratocumulus convection is considered as a vertical diffusion process with the eddy diffusion coefficients depending on the cloud water content, cloud fraction and the gradient of relative humidity at the top of the cloud.

Stratiform clouds are predicted in accordance with a cloud water equation including sources and sinks due to condensation/evaporation and precipitation formation both by coalescence of cloud droplets and sedimentation of ice crystals. Sub-grid scale condensation and cloud formation is taken into account by specifying appropriate thresholds of relative humidity depending on height and static stability.

The land-surface model considers the budget of heat and water in the soil, snow over land and the heat budget of permanent land and sea ice (Dümenil and Todini, 1992). The heat transfer equation is solved in a five-layer model assuming vanishing heat flux at the bottom. Vegetation effects such as interception of rain and snow in the canopy and the stomatal control of evapotranspiration are grossly simplified.

A detailed description of the model and a documentation of its performance has been presented by Roeckner et al (1992), Geckler et al (1994) and Arpe et al (1994).

For the experiments presented here, the model has been run in the so called "time-slice" mode: First a control simulation is carried out with prescribed climatological SST and present day CO_2 concentration ($1*CO_2$). Then the CO_2 concentration is doubled and the change of the SST at the time of doubling of CO_2 of a transient experiment done with a low resolution version of the model coupled to a realistic ocean

model (Cubasch et al, 1992) is added to the climatological SST ($2*CO_2$). In a third experiment the CO_2 concentration has been set to three times its present day level, and the change of the SST at the time of the tripling of CO_2 in the transient experiment has been added to the climatological SST ($3*CO_2$). All experiments have been run for 30 years and provide therefore an adequate sample for subsequent studies.

This time-slice method, as well as the same SST change data and the changes in the CO_2 concentration has been employed by Mahfouf et al (1994) and by Parey (1994). The dynamical aspects of the time-slice simulations with the ECHAM3 model and a comparison to the low resolution globally coupled ocean-atmosphere model (ECHAM1 + LSG) can be found in Perlwitz et al (1994).

3.0 Results

The model data are compared with the rainfall data after Legates and Willmott (1990) and data for the surface temperature after Jones and Briffa (1992a, 1992b).

Beside the regions defined in the IPCC 1990 report, Central and Northern Europe have been analysed (Fig.1). We considered only the land points.

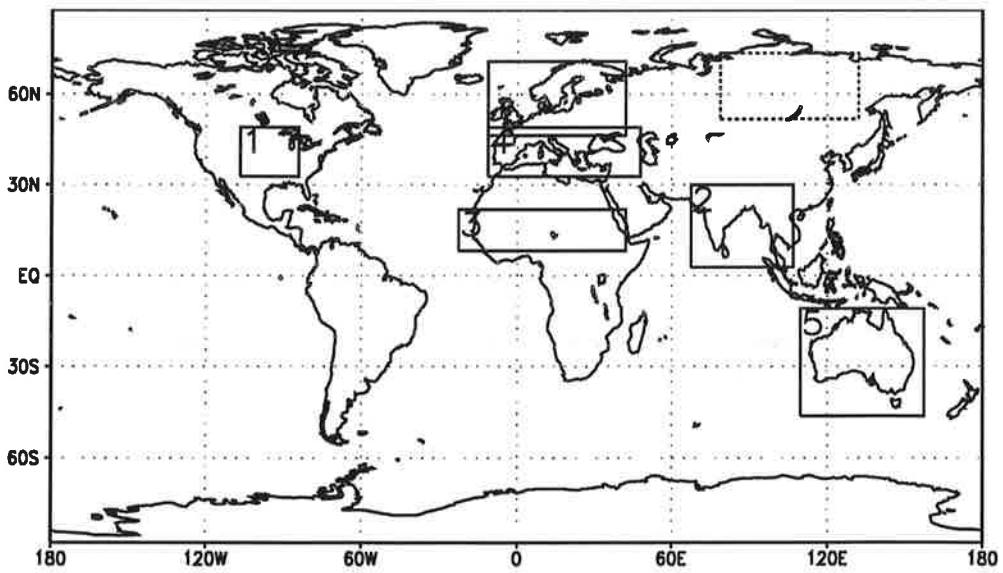

FIGURE 1. The six regions discussed in this study. Regions 1 - 5 represent the regions proposed by IPCC 1990. (Northern Asia is discussed only in section 3.1.3)

Table 1: The regions selected for this study

No.	boundaries	location	number of land- points in area	remarks
1	85^0 - 105^0 W, 35^0 - 50^0 N	Central North America	46	IPCC '90
2	70^0 - 105^0 E, 5^0 - 30^0 N	Southern Asia	69	IPCC '90
3	20^0 W - 40^0 E, 10^0 -20^0 N	Sahel	97	IPCC '90
4	10^0 W - 45^0 E, 35^0 - 50^0 N	Southern Europe	76	IPCC '90
5	110^0 - 155^0 E, 12^0 - 45^0 S	Australia	84	IPCC '90
6	10^0W - 40^0 E, 50^0 - 70^0 N	Central and Northern Europe	91	

These regions are only a subset of the regions actually analysed. To discuss all of them would exceed the sensible size of a paper. We therefore restrict ourselves to the regions of general interest and we only refer to other regions to deepen the insight into the problems.

3.1 Changes in the seasonal cycle

Two quantities are of primary concern for mankind and are among the most commonly measured, at least over land, i. e. precipitation and near surface temperature. Santer et al (1994) found in an analysis of transient climate change experiments with a low resolution model that the temperature has a high signal to noise ratio, the precipitation is quite noisy and a climate change in the precipitation is therefore more difficult to predict.

3.1.1 Changes in surface temperature

The annual cycle of the surface temperature (Fig. 2a) is simulated for Central North America in the 1*CO_2 simulation with the right amplitude, but with a warm bias of around 5 K in summer and winter. The temperature change is only marginal by going

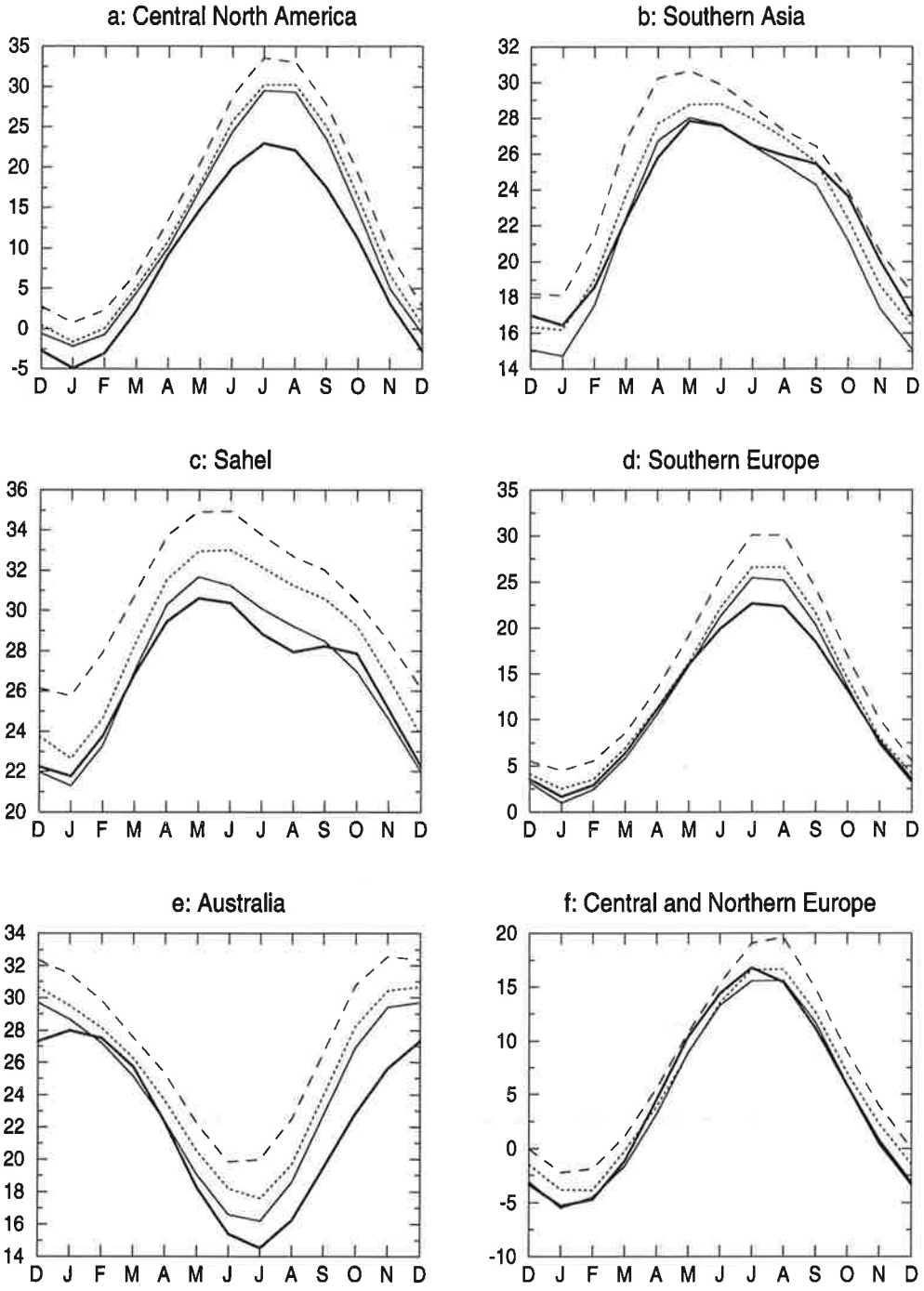

FIGURE 2. The annual cycle of the near surface temperature [°C] for the observation (bold solid) and the 1*CO_2 (thin solid), 2*CO_2 (dotted) and 3*CO_2 (dashed) integrations for Central North America (a), Southern Asia (b), the Sahel region (c), Southern Europe (d), Australia (e), and Central and Northern Europe (f).

from 1*CO_2 to 2*CO_2 and exceeds only in the autumn and winter season 1 K. With the 3*CO_2 experiment, a clear signal is established with an average above 3 K. In this experiment the annual cycle is altered with a minimum in spring and a maximum in late fall (longer Indian summer). The maximum in autumn is connected with an increased cloud cover, thus trapping the infrared radiation near the surface. In spring the cloud cover is reduced, allowing for more infrared cooling of the surface. The temperature changes for both (Fig. 3a), the 2*CO_2 and 3*CO_2 experiments, are significant. However, they are still smaller than the difference to the observation. The year to year variability does not increase significantly in either experiment.

In Southern Asia the observed annual cycle of the near surface temperature (Fig. 2 b) is in spring and summer comparable with observations, but during the other seasons too cold (ca. 2 K in December). The temperature change (Fig. 3b) for the 2*CO_2 experiment over Southern Asia is almost the same in every season, while in the 3*CO_2 simulation it has a marked intraseasonal variability with a maximum of 4.5 K in March and a minimum of only 2 K in autumn. The temperature change is correlated with the change in the solar radiation at the top of the atmosphere with 74% and with the solar radiation reaching the surface with 77%. The key to this phenomenon is the monsoon circulation. In March the conditions in this region are determined by flow from the north giving dry and clear sky conditions. In this case solar radiation passes almost unhindered to the surface, while the enhanced greenhouse effect directly warms the surface. During the pre-monsoon season (March) the radiative input at the surface is increased by up to 6 W/m^2 for the 3*CO_2 simulation. In the summer, more and thicker clouds due to the enhanced hydrological cycle reflect more solar radiation at the top of the atmosphere and absorb more solar radiation on their way to the surface. During the summer month, an average of about 14 W/m^2 less solar radiation reaches the ground in the 3*CO_2 simulation compared to the control simulation. Even though the thermal radiation is enhanced due to the greenhouse effect, the net radiation at the surface is reduced by about 2.5 W/m^2 during the summer month. The interannual variability does not change with increased greenhouse gas concentration.

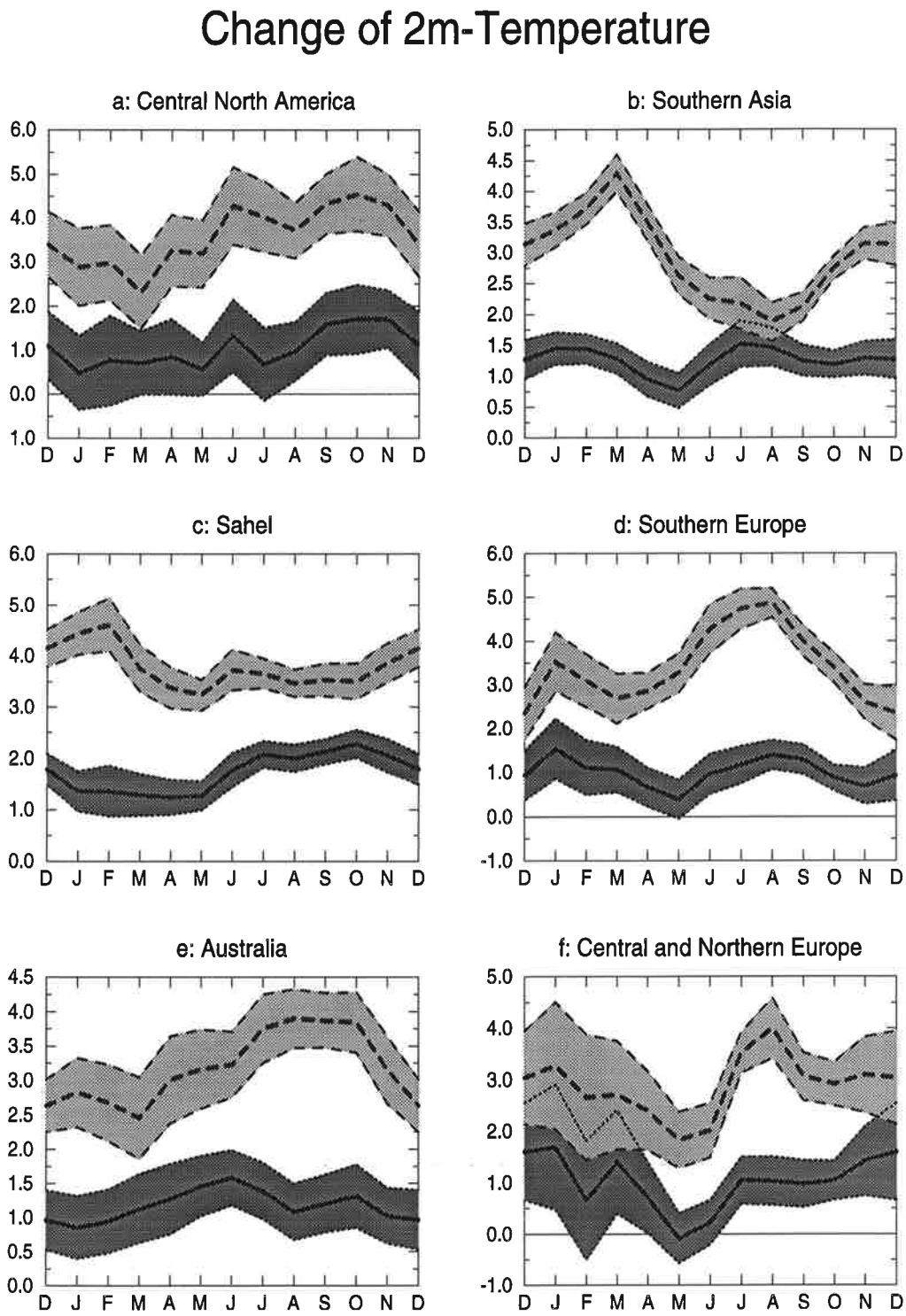

FIGURE 3. The annual cycle of the near surface temperature change [°C] for the $2*CO_2$ (dotted, dark shading) and $3*CO_2$ (dashed, light shading) integrations relative to the $1*CO_2$ experiment for Central North America (a), Southern Asia (b), the Sahel region (c), Southern Europe (d), Australia (e), and Central and Northern Europe (f). The shading indicates the confidence limits.

In the Sahel region, the observed seasonal change of the near surface temperature (Fig. 2 c) has about the same amplitude as in the model with deviations to observed below 2 K. A real jump in the temperature occurs in the Sahel region only by the 3*CO_2 experiment with more than 3.5 K on average (Fig. 3c), while with 2*CO_2 the warming is just between 1.5 and 2 K. The change in the season cycle is comparatively small and not consistent between the 2*CO_2 and the 3*CO_2 experiment. Again, the interannual variability is not significantly altered.

In Southern Europe (Fig. 2d), the observed seasonal cycle is simulated well in the model for all seasons with the exception of summer, where the simulated temperature is about 3 K too cold. Like in Central Northern America, the temperature change over Southern Europe in the 2*CO_2 experiment is only marginal and displays no distinct annual cycle. In the 3*CO_2 experiment, however, the temperature difference (Fig. 3d) rises from 2.5 K in winter to a maximum of 5K in late summer. The temporary minimum in May is caused by a decrease in the cloud cover and a decrease in the soil moisture. The gain of solar radiation at the surface is overcompensated by thermal radiation, thus in the mean the temperature is raised less than the annual average. In the subsequent month the solar radiation dominates the budget, while the greenhouse effect allows less thermal radiation to leave the atmosphere, thus leading to a temperature maximum, since the soil-moisture and the cloud cover conditions are almost unchanged compared to the control simulation. Again, the interannual variability is not significantly altered.

As in Southern Europe, the annual cycle of simulated temperature in Australia (Fig. 2e) has the minimum and maximum in about the right month as observed. The model is too warm in all seasons with the exception of southern hemisphere autumn. The largest deviations occur in southern hemisphere summer with differences of up to 4 K. The temperature increase (Fig. 3e) has only a marked seasonal cycle in the 3*CO_2 experiment, where it accelerates the Austral spring. Under 2*CO_2 condition the tem-

perature rise is seasonally almost independent and only about 30% to 40% of the $3*CO_2$ value. Again, the interannual variability is not significantly altered.

In Central and Northern Europe, the seasonal temperature cycle is simulated almost perfectly (Fig. 2f). In the $2*CO_2$ as well as in the $3*CO_2$ experiment the change of the temperature is significant and counteracts the seasonal cycle, i. e. the temperature change is much larger in winter than in summer, where in the $2*CO_2$ simulation hardly any temperature change can be found. In this simulation, only in the winter season the temperature change exceeds 1K. The variability is not significantly altered.

In some regions the temperature change is for both climate change simulations still smaller than the deviation of the simulation to observations. The predicted climate change for the $2*CO_2$ experiment generally only amounts to about 30% to 40% of the one obtained by the $3*CO_2$ experiment. This can be attributed to the cold start phenomenon (Cubasch et al, 1995; Hasselmann et al, 1992). It is caused by the fact that the start of the transient experiment was 1985, not at the beginning of the industrial burning of fossil fuel ca. 1750. Therefore all the warming between 1750 and 1985 has been neglected, which causes a delay in the warming of this experiment. While the climate change simulated by the $2*CO_2$ experiment hardly displays much seasonal variability, the $3*CO_2$ run exhibits in many regions a clear annual signal. The forcing of the $3*CO_2$ simulation appears to be strong enough to trigger off a number of positive feedback mechanisms, which reinforce the signal and alter the seasonal cycle. In fact the result of this $3*CO_2$ experiment rather resembles the $2*CO_2$ simulations with mixed-layer models. This is not that surprising, since transient simulations have, at the time of CO_2 doubling only achieved about 60% of their equilibrium warming (Cao et al, 1991; IPCC, 1992). Assuming a response time of the coupled model of about 35 years (Cubasch et al, 1995), it will have obtained the amplitude of the CO_2 equilibrium response at around 100 years of simulated time, just the time, when its transient forcing has reached the $3*CO_2$ mark.

A change in the variability can generally not be detected. As has been stated by Bengtsson et al (1994) the model underestimates the natural variability in the tropics when driven by climatological sea-surface temperatures. Its sensitivity towards changes in the variability might therefore not addressable.

3.1.2 Changes in precipitation

A thorough investigation of the hydrological cycle in the ECHAM3 model has been carried out by Arpe et al (1994). It indicates that the uncertainties in the observations cause severe problems in the validation of the model results. The model simulates the precipitation mainly within the brackets of uncertainty of the observations. Instead of going through the exercise of comparing the model results to all available observations again, we restrict ourselves to the climatology of Legates and Willmott (1987) bearing in mind the large uncertainty inherent in this dataset.

The simulated precipitation over Central North America completely misses the peak in summer (Fig. 4a). The mean value is only about 50% of the observed amount. The precipitation does not significantly change in Central North America in any of the climate change simulations. Differences of a maximum of 20% still fall within the interannual variability of the control simulation (Fig. 5a). The interannual variability is not significantly altered either.

The precipitation over Southern Asia (Fig. 4b) has a marked seasonal cycle with a minimum in early spring (the winter monsoon) and a maximum in late summer. The annual cycle of precipitation is simulated quite well over Southern Asia, even though the maximum during the summer monsoon season is underestimated about 30%. This, of course, also drags the mean simulated value below the observed mean.

Under the $2*CO_2$ conditions this situation is hardly altered (Fig. 5b), and changes are barely significant. Under the $3*CO_2$ conditions, the precipitation in the monsoon season increases by 10%. It has already been stressed by Lal et al (1994) that the enhanced hydrological cycle results in an increase of the monsoon precipitation over

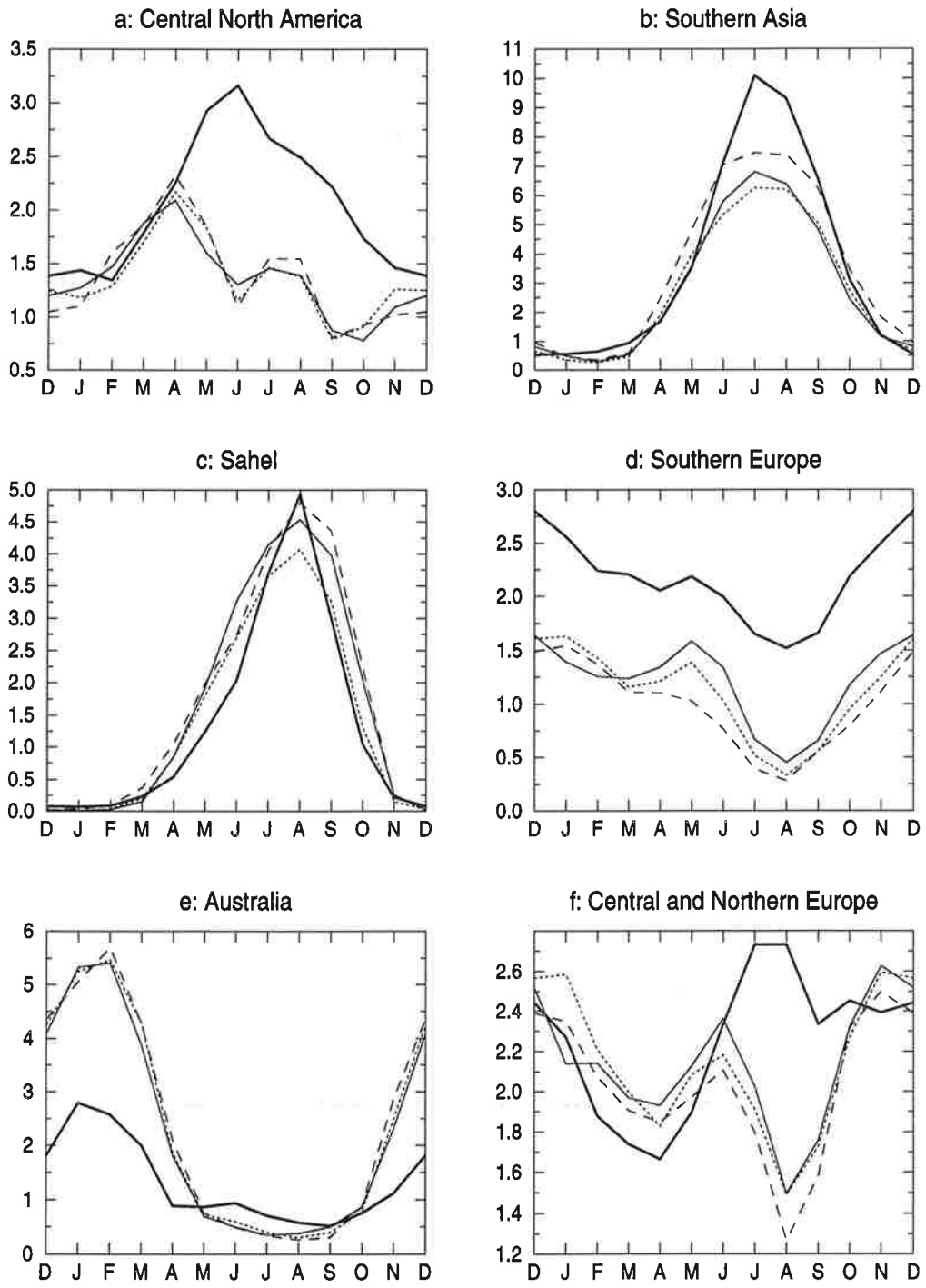

FIGURE 4. The annual cycle of the precipitation [mm/d] for the observation (bold solid) and the 1*CO_2 (thin solid), 2*CO_2 (dotted) and 3*CO_2 (dashed) integrations for Central North America (a), Southern Asia (b), the Sahel region (c), Southern Europe (d), Australia (e), and Central and Northern Europe (f).

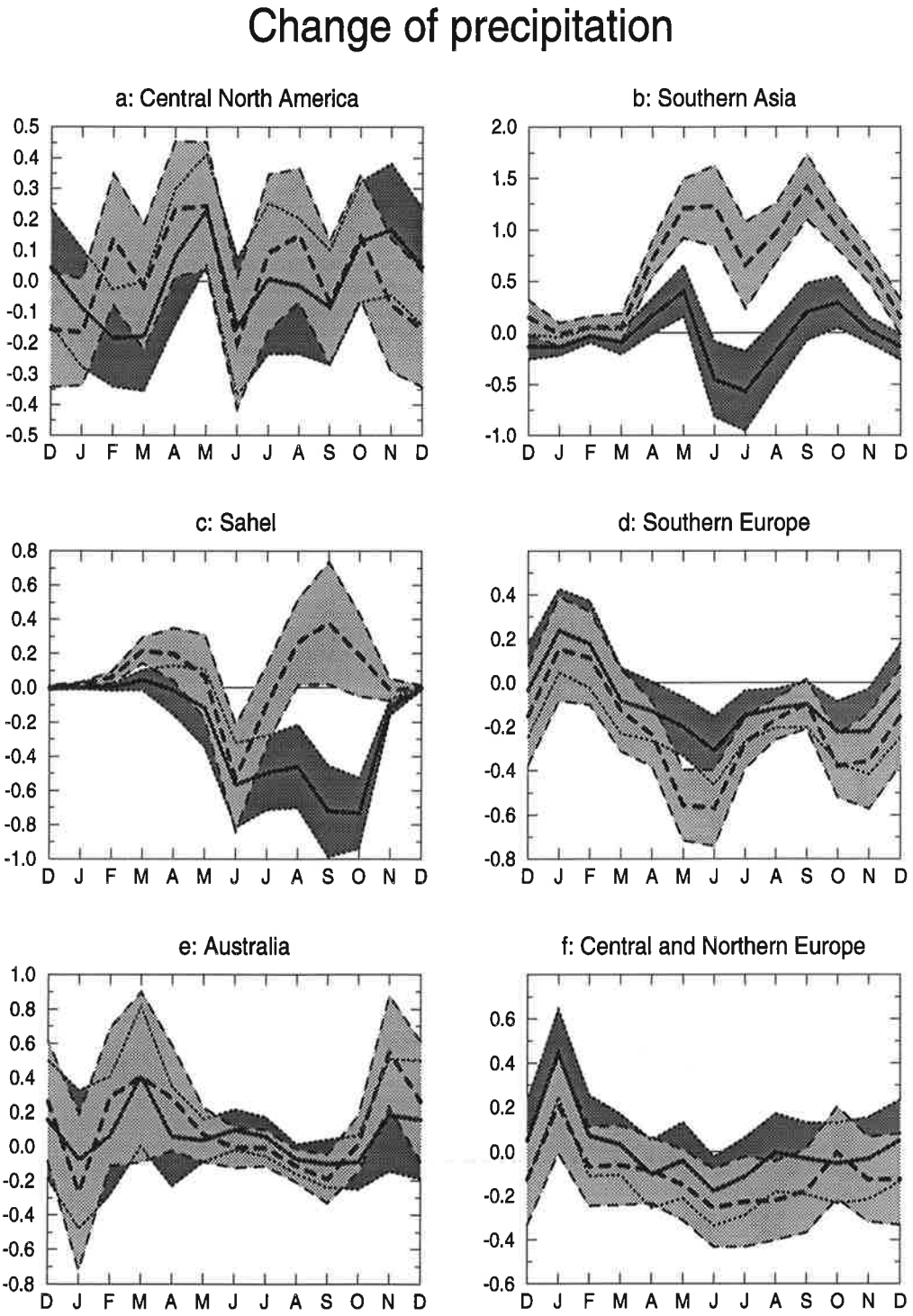

FIGURE 5. The annual cycle of the precipitation change [mm/d] for the 2*CO_2 (dotted, dark shading) and 3*CO_2 (dashed, light shading) integrations relative to the 1*CO_2 experiment for Central North America (a), Southern Asia (b), the Sahel region (c), Southern Europe (d), Australia (e), and Central and Northern Europe (f). The shading indicates the confidence limits.

India. The interannual variability is not significantly influenced by the greenhouse gas concentration.

Contrary to the temperature, the annual cycle of precipitation, its mean and its amplitude, are well simulated in the Sahel region (Fig. 4c). The change of precipitation is very inconsistent among the experiments. While the $2*CO_2$ experiment predicts a decrease of 40% during summer and autumn, the $3*CO_2$ experiment predicts a 20% increase (Fig. 5c). The variability increases during the dry season (December to March) in the $3*CO_2$ experiment. Even though the statistical test suggests that this increase is significant, the low absolute amount during this season casts some doubt about the sense of this test under these circumstances.

The annual cycle of the precipitation over Southern Europe (Fig. 4d) is simulated well, however the absolute amount is underestimated by a factor of two. The precipitation is increased during the winter season in both climate change experiments, but it is decreased during the summer season (Fig. 5d). The seasonal cycle of precipitation is therefore enhanced.

There are indications that the variability during the summer season is enhanced in both climate change simulations.

While the winter precipitation over Australia (Fig. 4e) has been simulated well, the steep increase in spring and autumn simulated by the model cannot be found in the observations. The annual mean is therefore overestimated. No clear signal can be identified for the precipitation change (Fig. 5e). It is as well as under $2*CO_2$ as well as $3*CO_2$ conditions not significant and displays no seasonal cycle. No unequivocal significant change in the variability of precipitation can be found under the changed climate conditions.

The observed summer precipitation of Central and Northern Europe shows a relative maximum while the model simulates a minimum. During the other seasons the observed and simulated values agree quite well. The mean value is underestimated.

Under climate change conditions, the models predict on average a drying, which reaches its maximum during the (already unreasonably dry) summer season, but which is not statistically significant. This decrease of precipitation is slightly higher in the $3*CO_2$ compared to the $2*CO_2$ experiment. The variability is not influenced by the climate change conditions.

The analysis of the seasonal precipitation shows that this parameter is only poorly simulated. The change of precipitation confirms the statements made by Santer et al (1994) that precipitation has a low signal-to-noise ratio, because it does not show an unequivocal sign. Even the tripling of CO_2, which has a large impact on the near surface temperature, did not influence precipitation in a distinct way, with the exception of Southern Asia and the Sahel. Generally the deviation in the precipitation simulation compared to observations is larger than the predicted climate change

3.1.3 The combined change of precipitation and surface temperature

To investigate the combination of changes of temperature and changes of precipitation in a region, we have plotted for all regions the changes of precipitation versus the changes of temperature of every month. Fig. 6a shows the results for Northern Asia, which has been selected, because it has a strong negative correlation between precipitation and temperature change (i. e. in the month with the largest temperature increase the precipitation has s gained its maximum rise as well), and for Southern Asia (Fig. 6b), which has a strong negative correlation. These two regions are prime examples of the two possible correlations between changes of temperature and precipitation. It is not very distinct in the experiments with the $2*CO_2$, but can clearly be seen in the experiments with the $3*CO_2$ concentration.

The mechanisms of this different behavior can be explained as follows. In northern Asia (not shown) the temperature increase is largest in late fall and early winter, since the global warming delays the onset of snowfall. At the same time the precipitation increase is at a relative maximum, because the increased temperature allows more humidity to be transported northwards. This rainfall is connected with a substantial

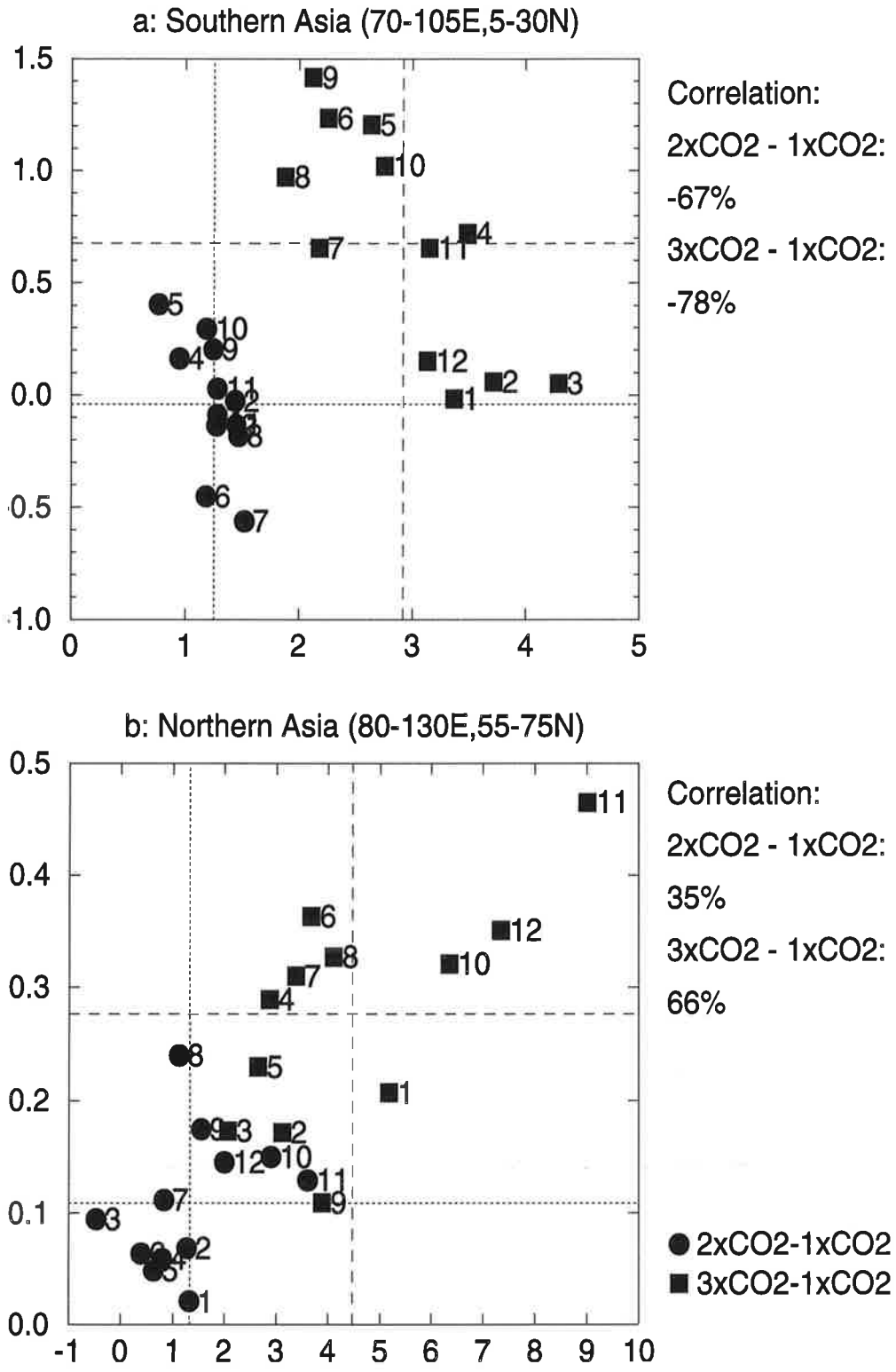

FIGURE 6. The monthly ratio between temperature change [^{o}C] and the precipitation change [mm/d] for the 2*CO_2 and the 3*CO_2 experiment for Southern Asia (a) and Northern Asia (b). The numbers beside the circles and squares are representing the months.

increase of the cloud cover, trapping the longwave radiation at the surface, while reflecting little shortwave radiation at the top of the atmosphere, since the radiative input in winter is low. The net radiative gain at the surface is 3 W/m^2 for the winter season. In spring and summer the higher snow depth due to the increased winter precipitation takes more time to melt, and more snow is removed, which dampens the warming, and increases of the hydrological cycle.

In southern Asia the temperature increases predominately in the seasons with the minimum percentage of the annual rainfall directly due to the greenhouse effect (c. f. section 3.1.1) In the rainy season the rainfall increases due to the increased hydrological cycle. This is connected with an increased cloudiness. The increased albedo allows less solar radiation to reach the ground. Furthermore, the increased soil wetness counteracts any direct warming.

The combined precipitation-temperature change in other regions can be explained by similar mechanisms, but they rarely are as distinct as in Southern and Northern Asia.The global correlation between temperature- and precipitation change has been displayed in Fig. 7 for the $3*CO_2$ experiment. Since one is interested only in a time consistent signal, i. e. an observation is only sensible in those regions, where the correlation between temperature- and precipitation change has the same sign with any increase of CO_2, the correlation has only been displayed for those points, where it has the same sign for both, the $2*CO_2$ and $3*CO_2$ experiment. Polar regions clearly belong to the category where the seasonal temperature change is positively correlated with an increase in precipitation, while tropical regions and part of the subtropics show a negative correlation. For large areas, particularly in the mid-latitudes, no correlation can be found, which is consistent between the $2*CO_2$ and $3*CO_2$ experiment. The strong correlation in certain regions of the globe, however, makes the combination between temperature- and precipitation change an interesting quantity to evaluate in observations.

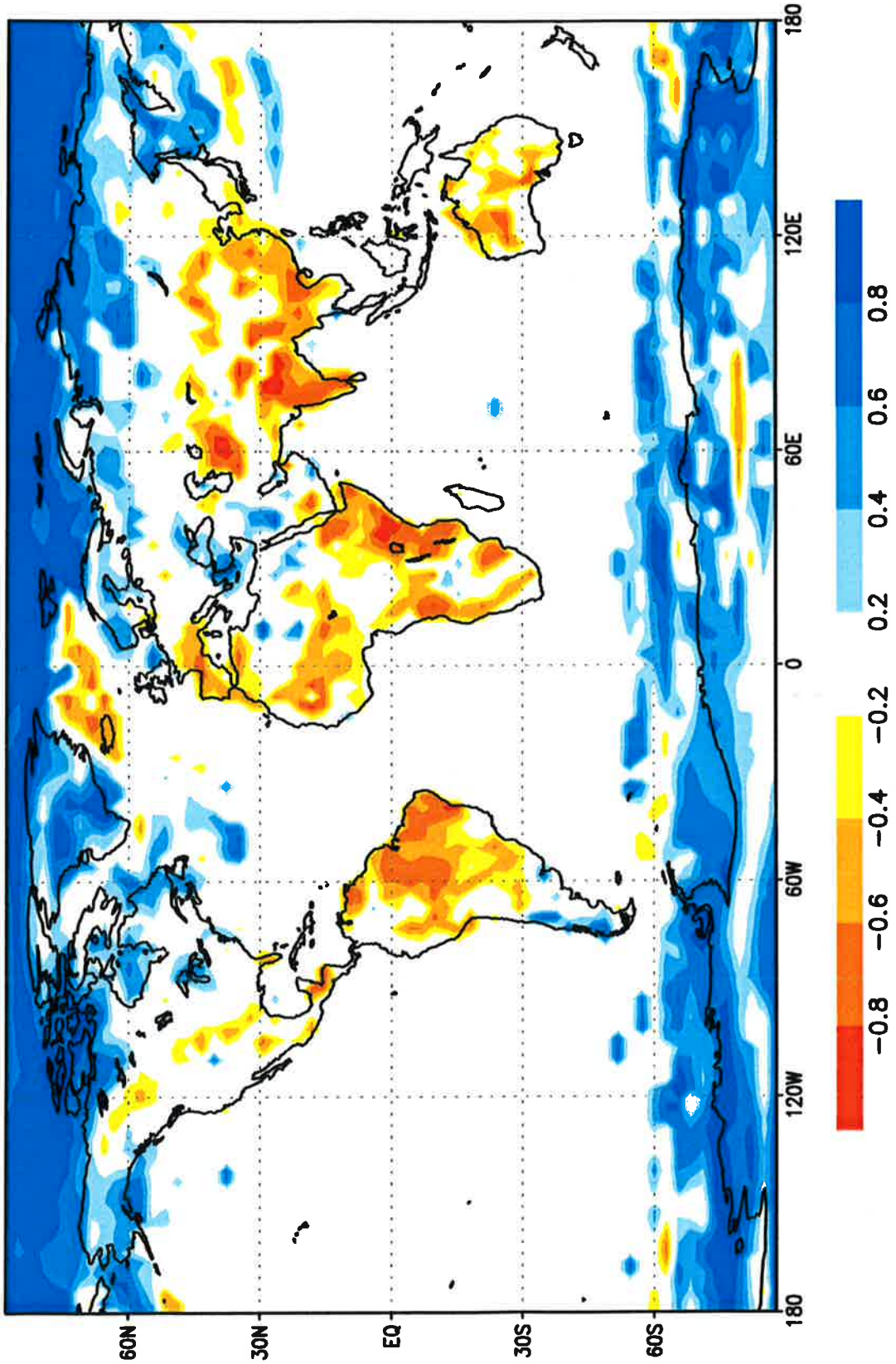

FIGURE 7. The latitudinal distribution of the correlation between temperature change and precipitation change (annual mean) for the 3*CO_2 experiment. Only those points have been plotted, where the correlation of the 2* CO_2 and 3*CO_2 integration has the same sign and the range of temperature change is at least 1°C.

3.2 Daily temperature contrast change

Karl et al (1994) have stressed that there is some indication that the observed global warming is partially caused by a higher increase of the daily minimum temperature than that of the daily maximum temperature. This causes a decrease of the daily amplitude of temperature. Possible reasons for this effect might be changes in cloudiness and/or in the aerosol distribution.

This phenomenon can also be seen in the model simulations, but not equally strong in all regions: Contrary to the changes in the mean values, the changes in the daily temperature contrast over North America (Fig. 8a, 9a) are more pronounced for the $2*CO_2$ experiment than in the $3*CO_2$ simulation. In all seasons except for late summer/early fall the daily temperature contrast is diminished. As the change in the daily temperature range is small and does not even have the same sign for the $2*CO_2$ and the $3*CO_2$ experiment, it is difficult to find the physical mechanisms behind it. The signal is certainly not as strong in the model as the observations suggest (Karl et al, 1993). This might, however, also be connected by an unfortunate choice of the IPCC region, which leaves out most of the North American continent.

Southern Asia (Fig. 8b, Fig. 9b) has a strong change of the daily temperature contrast at the $3*CO_2$ experiment. This change has a pronounced seasonal cycle as well. It is diminished by almost 1.5 K in late fall. The minimum temperature has risen more than the maximum temperature, which is caused by the higher soil moisture due to the enhanced hydrological cycle in this particular region (c. f. section 3.1.2) and therefore with an increased amount of water-vapor and clouds. In the Sahel region (Fig. 8c, 9c) the change of the daily temperature contrast is not unequivocal. In the $2*CO_2$ experiment the contrast increases in summer and autumn, while in $3*CO_2$ it decreases in almost every season. The change in precipitation might be the key to this inconsistent behavior: In the seasons with the strongest difference between $2*CO_2$ and $3*CO_2$ (summer and fall) the rain increases with $3*CO_2$ and decreases with $2*CO_2$.

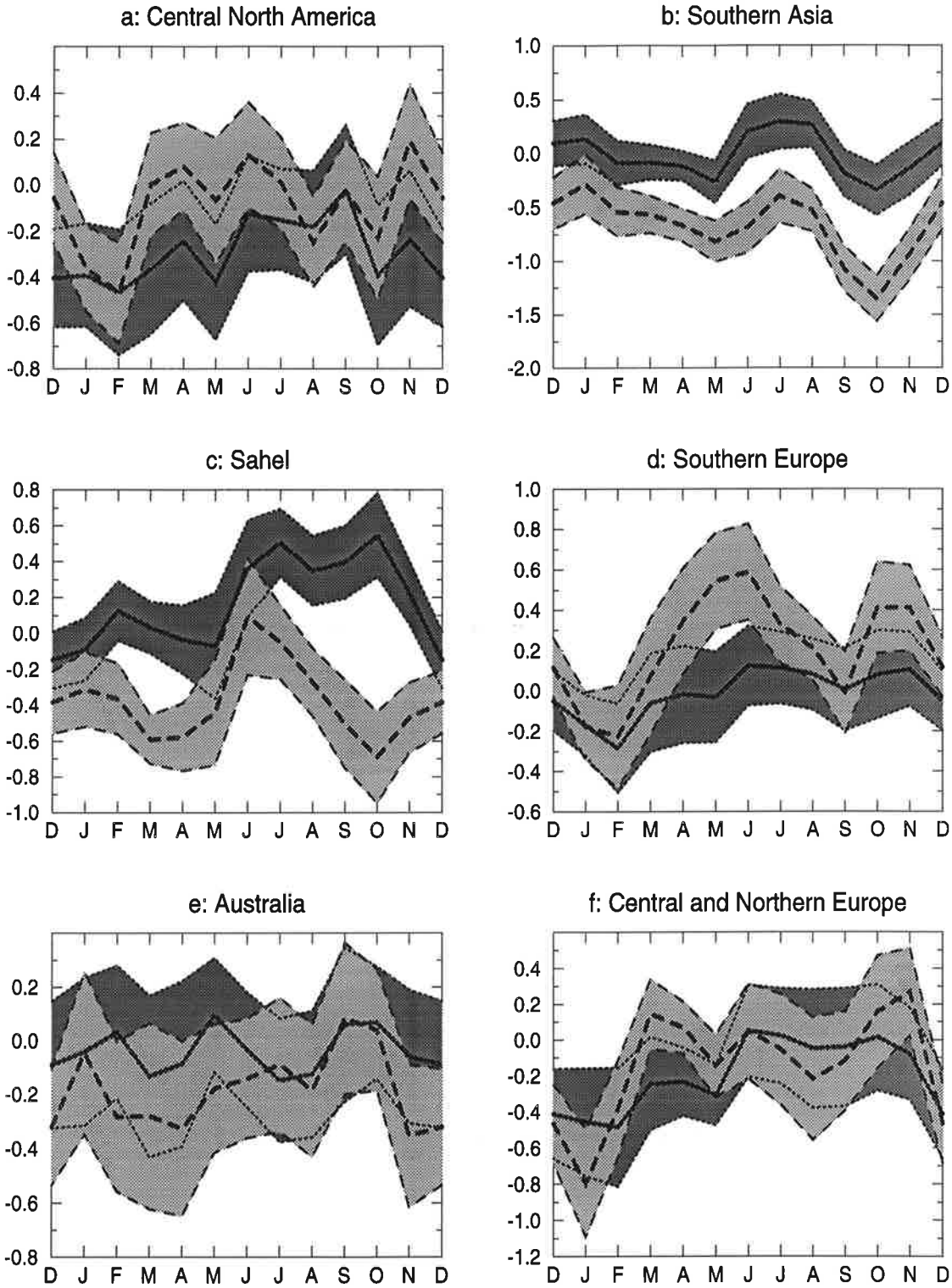

FIGURE 8. The change of the annual cycle of the daily temperature contrast [^{o}C] for the 2*CO_2 (dotted) and 3*CO_2 (dashed) integration relative to the 1*CO_2 experiment for Central North America (a), Southern Asia (b), the Sahel region (c), Southern Europe (d), Australia (e), and Central and Northern Europe (f). The shading indicates the confidence limits.

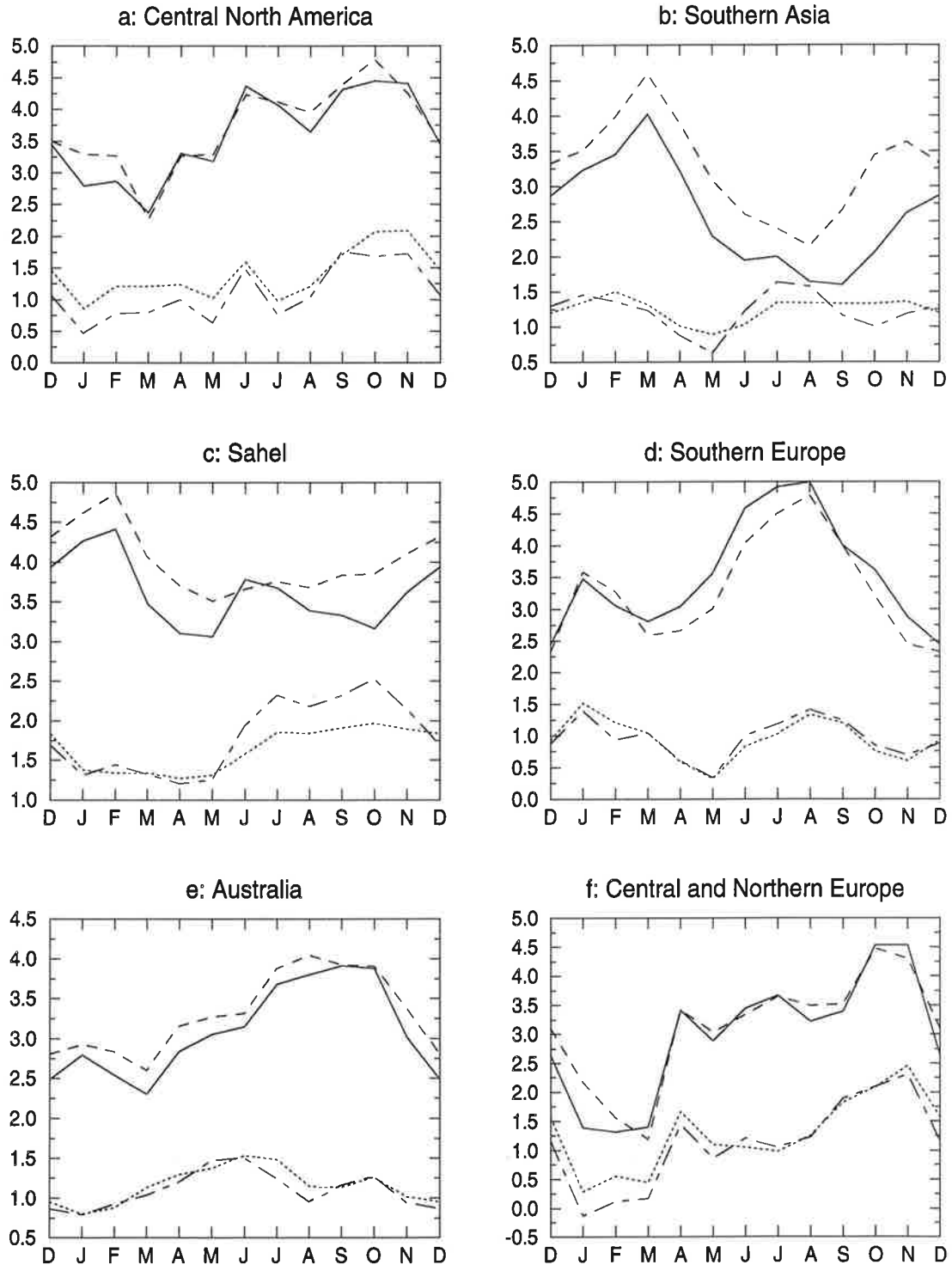

FIGURE 9. The change of the annual cycle of the minimum and maximum temperature [°C] for the $2*CO_2$ and $3*CO_2$ integration relative to the $1*CO_2$ experiment for Central North America (a), Southern Asia (b), the Sahel region (c), Southern Europe (d), Australia (e), and Central and Northern Europe (f). Solid: $3*CO_2$ minus $1*CO_2$, maximum temperature; dashed: $3*CO_2$ minus $1*CO_2$, minimum temperature; dash-dot: $2*CO_2$ minus $1*CO_2$, maximum temperature; dotted: $2*CO_2$ minus $1*CO_2$, minimum temperature.

In southern Europe (Fig. 8d, 9d) the change in the daily temperature contrast increases in the 3*CO_2 experiment, particularly in summer, while it stays almost unchanged in the 2*CO_2 experiment. In the 3*CO_2 experiment, this can be linked to cloudiness: In summer the cloudiness decreases and allows during daytime more solar radiation to reach the surface. At the same time the soil-moisture has become so low that the radiation is directly converted into a temperature increase. It would be interesting to see if this different behavior of the daily temperature contrast can be found in observations as well, but so far observations for Europe has only been analysed on a single location (Karl et al, 1993; Bücher and Dessens, 1991). On this spot (Pyrenees) a lowering of the contrast has been observed. This does, however, not contradict the model results, since this observing station is located in a region, where the model gives no definite answer, and a doubling of CO_2 has not yet been reached in the real atmosphere. Cao et al (1991) find in a simulation with a mixed-layer model that for CO_2 doubling over Europe the diurnal temperature range is increased as well, but only in spring.

The change of the daily temperature contrast over Australia (Fig. 8e, 9e) is, at least for the 2*CO_2 experiment, quite erratic, while a decrease can be found, particularly for the Austral summer, in the 3*CO_2 run. The erratic nature of this change makes it difficult to attribute it to a physical mechanism.

The temperature contrast does not increase on average over Central and Northern Europe (Fig. 8f, 9f), because the signal is rather unequivocal. This is caused by the peculiarity of the region selected. Taking both, Central and Northern Europe separately, one finds that in Central Europe the contrasts increases, while in Northern Europe it rather decreases (Fig. 10)

This Fig. 10 shows the regions, where the daily temperature contrast is changed in the 3*CO_2 experiment, but only, if the change of the 2*CO_2 experiment has the same sign, and only, if the change is statistically significant. Only in these regions an analysis of this quantity is advisable. It can be seen that in the annual mean in almost all land regions of the globe, with the notable exception of middle and southern Europe and

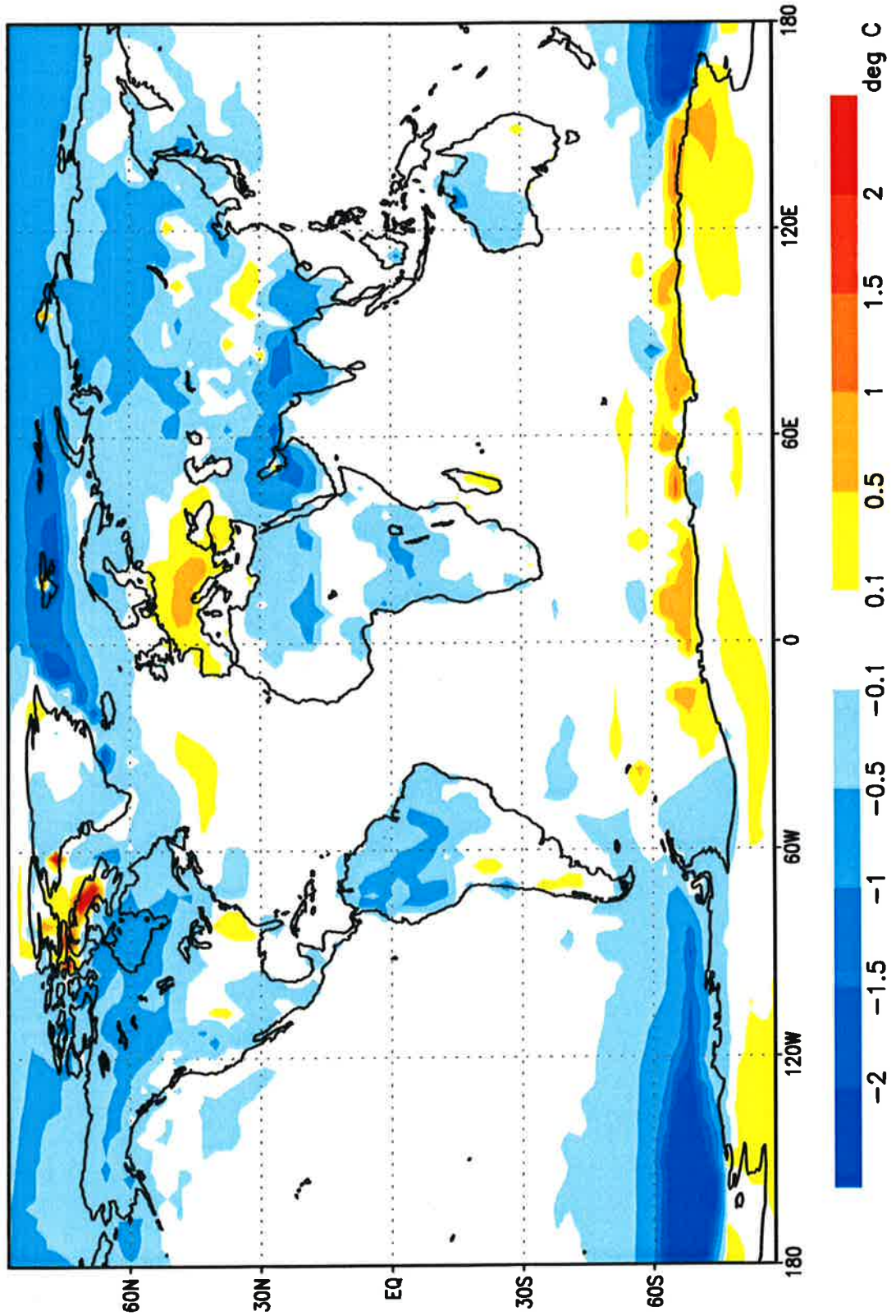

FIGURE 10. The regional distribution of the change of the annual mean difference between minimum and maximum temperature for the 3*CO_2 integration relative to the 1*CO_2 experiment. Regions, where the 2*CO_2 and 3*CO_2 simulation do not show the same trend or where the changes are not significant, have been blanked out.

Antarctica, there is a clear tendency for a diminished contrast. This is a stable pattern for all seasons. The Arctic undergoes a strong seasonal change with an increase in spring and a strong decrease in fall. This is related to the changed ice melt /ice formation in these transition seasons.

The change of the daily temperature contrast is strongly linked with the change in the total cloud cover, as has been found in observations in the US (Karl et al, 1993) and in the soil moisture (c.f. Table 2). More clouds or more soil moisture lowers the radiative cooling at the surface at night and allow less warming during daytime, and therefore causes a smaller minimum-maximum difference. The only exception is region No. 1 (Central North America). The low correlation in this area can be explained by the poorly defined seasonal cycle of the change of the daily temperature contrast.

Table 2: Correlation of the annual cycle of the daily temperature contrast change for 3*CO_2 (in brackets for 2*CO_2) with the one of the cloud cover and the soil moisture change.

No.	region	cloud cover change [%]	soil moisture change
1	Central North America	-28 (1)	-47 (-50)
2	Southern Asia	-92 (-87)	-78 (-47)
3	Sahel	-84 (-86)	-85 (-88)
4	Southern Europe	-86 (-51)	-73 (-43)
5	Australia	-85 (-54)	-75 (-92)
6	Central and Northern Europe	-70 (-61)	-63 (-23)

3.3 Changes in the precipitation intensity

To estimate the change in the rain intensity, the daily data have been scanned for the rain amount per 24 h interval, which are then separated into classes (>1, > 2, >5, >10, >20, >100 [mm/day]), and then added for every season.

Focussing on the IPCC regions, Fig. 11 shows the change of the precipitation classes for all seasons for the control, 2*CO_2 and the 3*CO_2 simulations. The height of each

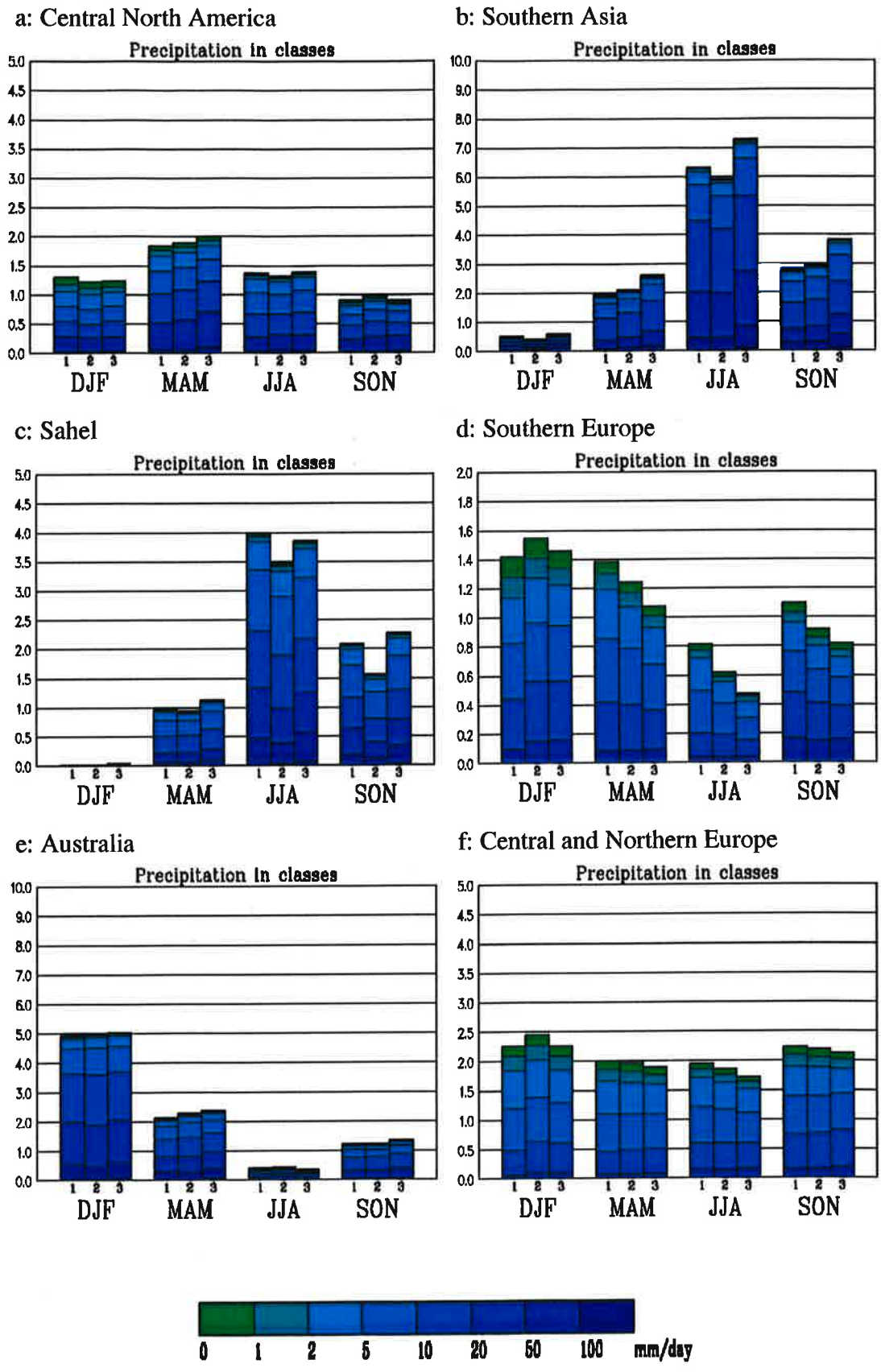

FIGURE 11. The seasonal distribution of precipitation intensity for the 1*CO_2, 2*CO_2 and 3*CO_2 integrations for Central North America (a), Southern Asia (b), the Sahel region (c), Southern Europe (d), Australia (e), and Central and Northern Europe (f).

column gives the total precipitation for every season. The share of each of the precipitation classes to the total amount is shown via the subdivisions of the columns. The uppermost box represents the class with the smallest precipitation-intensity.

As mentioned before the precipitation amount over Central North America (Fig. 11a) does not change significantly. It is, however, interesting to note that the rain intensities alter significantly. The class 50-100 mm/day has increased its share on the total precipitation in every season while the share of the rain classes below 10 mm/day stay the same ore even decrease under 3*CO_2 conditions in every season. Over southern Asia (Fig. 11b) particularly the rainfall in the summer monsoon season is increased, again by an increase in the high intensity events. This trend is systematic in the 2*CO_2 and 3*CO_2 experiments. It is interesting to note that in autumn too the severe rain-events increase. In the 3*CO_2 experiments even days with precipitation of more than 50 mm/day emerge, which are not present in the control simulation. In the Sahel region (Fig. 11c) most of the precipitation falls in summer and autumn. The change is not unequivocal, but again, there exits a tendency to increase the strong rain events at the 3*CO_2 experiment. Southern Europe experiences, with the exception of the winter season, less precipitation under increased CO_2 concentration conditions (Fig. 11d). The days with intense rain stay about the same or increase marginally. The decrease of overall rainfall can mainly be attributed to a decrease of the weak and medium intensity classes. Australia, as mentioned before, does not show a distinct change of the precipitation (Fig. 11e). There is a clear indication, that the number of days with high rain intensity increases while the number of days with a low rain intensity decreases. A similar result has been obtained by Whetton et al (1993), who analyses the change in rainfall intensity over Australia simulated by a number of equilibrium experiments. In Central and Northern Europe (Fig. 11d) the total rainfall decreases. The heavy rainfall events increase, particularly in the autumn.

Fig. 12 displays those regions of the 3*CO_2 experiment, where the heavy rain (>10 mm/day) is changed significantly (t-test) and has the same sign as in the 2*CO_2 experiment.

Only over oceanic regions the heavy precipitation decreases, while over large areas of the globe, particularly over the regions with tropical rain forest it increases. Since regions like the northern US, Canada and Northern Europe have long records not only of the rainfall amount, but also of the rainfall intensity, an analysis of this quantity for these regions might lead to a detection of the climate change.

3.4 Changes in the frequency of droughts

To get a more detailed view into the frequency of consecutive dry days (precipitation < 0.1 mm/d), 11 classes depending on the number of consecutive dry days have been defined. The classes are: 1 to 10, 11 to 20, 21 to 30, 31 to 60, 61 to 90, 91 to 120, 121 to 150, 151 to 180, 181 to 270, 271 to 360, and >360 days without precipitation. The simulated years have been scanned for these dry spells and every dry period has been classified. The frequency has been normalized by the total number of days analysed.

In Central North America (Fig. 13a) the total number of dry days increases with increased CO_2 concentration. This increase is mainly caused by an increase of very long dry periods. In the 30 year period analysed on would have only a 1% probability of a drought of more than 3 month, while in the 3*CO_2 experiment this chance is doubled.

In Southern Asia (Fig. 13b) the number of really dry days is actually decreasing in the 3*CO_2 experiment, and so is the probability of very long dry spells. In the Sahel region (Fig. 13c) the number of dry days stays roughly the same, and no marked shift towards longer dryer episodes can be found. Over Southern Europe (Fig. 13d) the probability of a longer dry spell increases with increased CO_2 concentration, particularly in the 30-60 day class interval. Australia (Fig. 13e) does not show any marked trend in the change of dry days. This is caused by combining regions with an increase of dry days

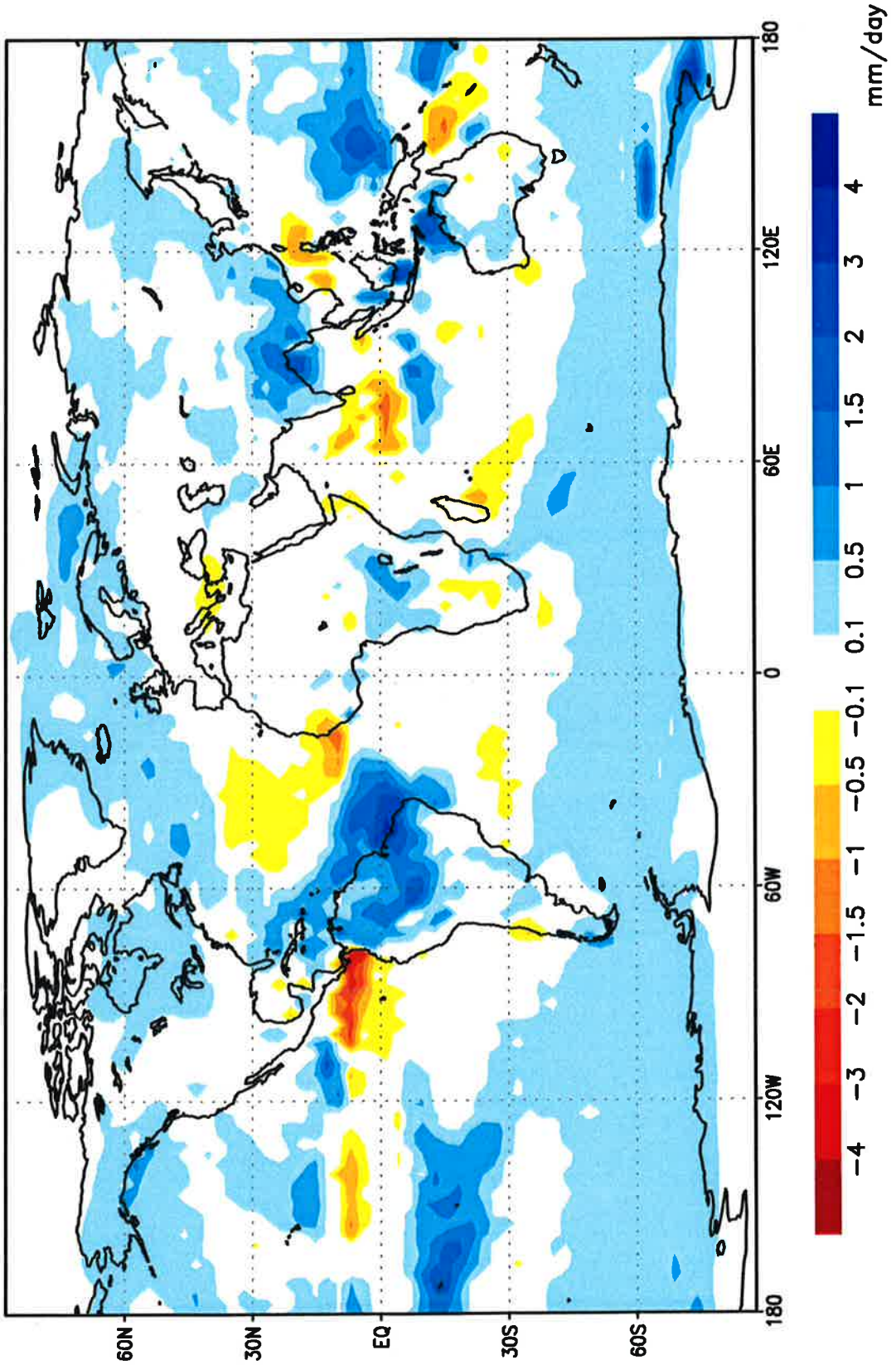

FIGURE 12. The regional distribution of the annual mean change of heavy rain (>10 mm/day) for the 3*CO_2 integration relative to the 1*CO_2 experiment. Regions, where the 2*CO_2 and 3*CO_2 simulation do not show the same trend or where the changes are not significant, have been blanked out.

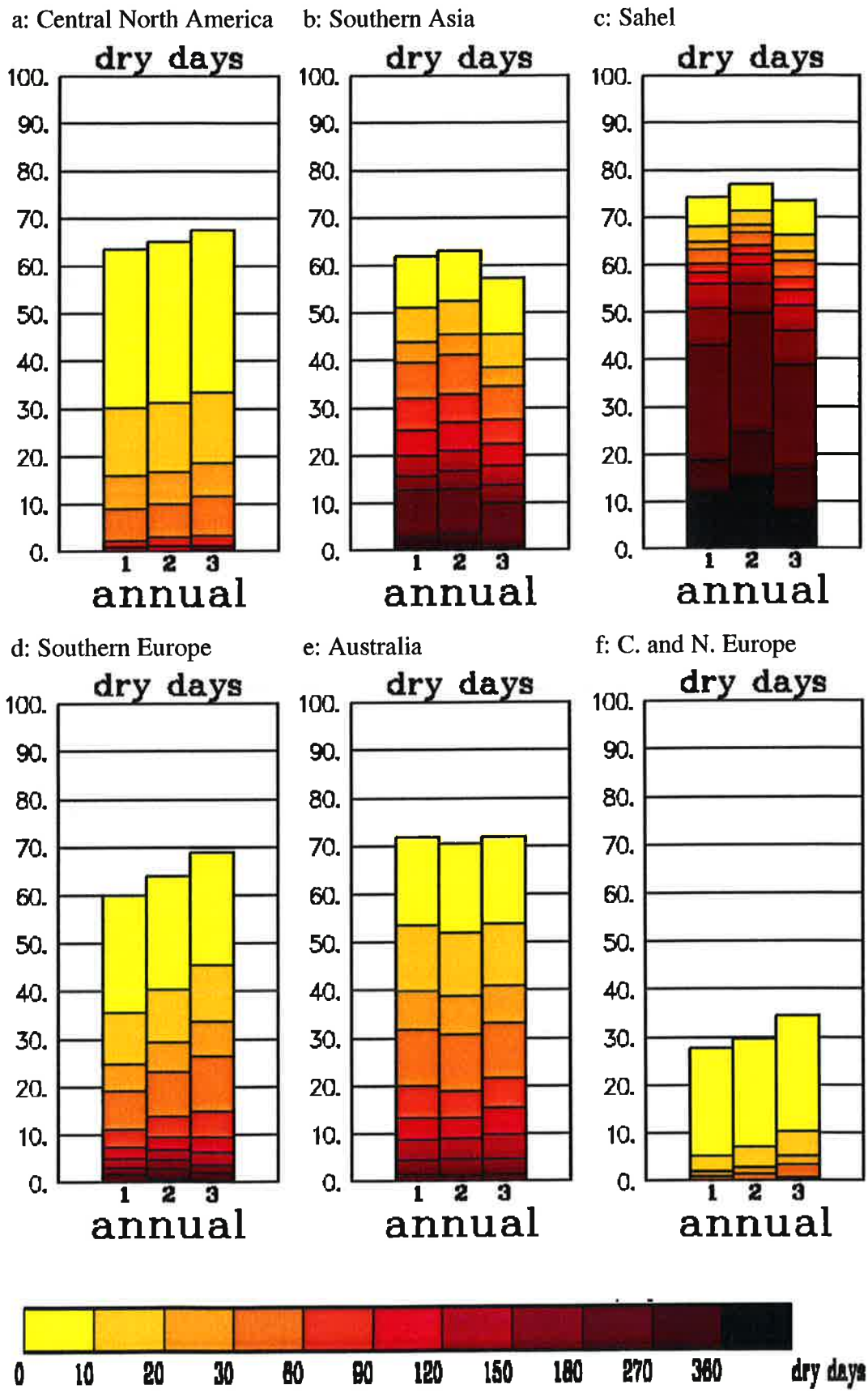

FIGURE 13. The annual mean distribution of consecutive dry days for the 1*CO_2, 2*CO_2 and 3*CO_2 integration for Central North America (a), Southern Asia (b), the Sahel region (c), Southern Europe (d), Australia (e), and Central and Northern Europe (f).

in the southern part of Australia with regions of an decrease of dry spells in northern Australia. Over Central and Northern Europe (Fig. 13f) a clear trend can be found towards more dry days and longer dry spells.

To obtain a global overview of the absolute number of dry days combined by their time distribution, we computed the "average waiting time for the next precipitation" (or expectation of storm- interarrival time) on a randomly chosen day. The significance of this quantity can be explained by an example: Let us consider two gridpoints, both of which have 50% rainy days within one year. In the first grid point it rains exactly every second day, while in the other 180 dry days are periodically followed by 180 rainy days. In the first case the waiting for rain time is $0.5 \times 1 + 0.5 \times 0 = 0.5$ days, but in the second case it is $\frac{1}{360} \times 180 + \frac{1}{360} \times 179 + \frac{1}{360} \times 178 + \ldots + \frac{1}{360} \times 1 + \frac{180}{360} \times 0 = 45.25$ days. The "average waiting time for the next precipitation" is therefore a measure for the length of dry spells. The change of this quantity has been displayed in Fig. 14 for the 3*CO_2 experiment, but again only for those points, where the sign for the 2*CO_2 and the 3*CO_2 experiment coincides. The "average waiting time for the next precipitation" is increased significantly in the midlatitudes, while it is decreased in the tropics and polar regions.

4.0 Discussion

The model displays substantial inconsistencies in simulating the observed climate of the specific regions studied here. The increase of the resolution to T42 compared to the T21 resolution used for the transient experiment alleviates some of the problems, but the model is far from perfect (Perlwitz et al, 1994; Arpe et al, 1994). The model simulates in most regions the annual mean climatology realistically with deviations rarely exceeding 3 K. In some regions, the model deviations are larger than the simulated change for the climate change scenarios. Thus, all results have to be treated with caution.

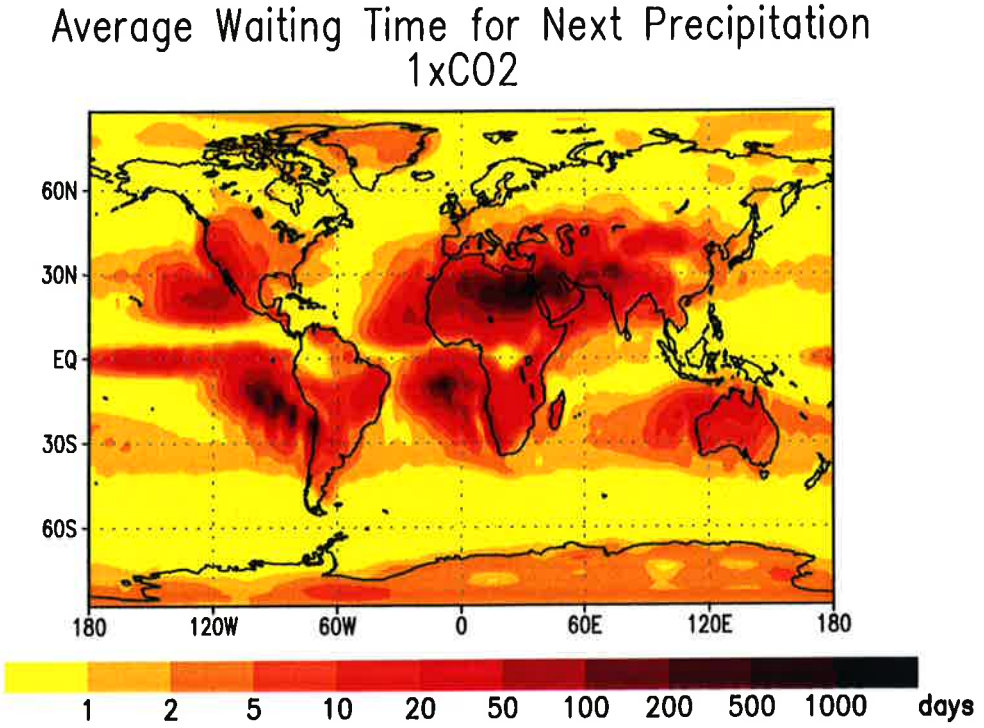

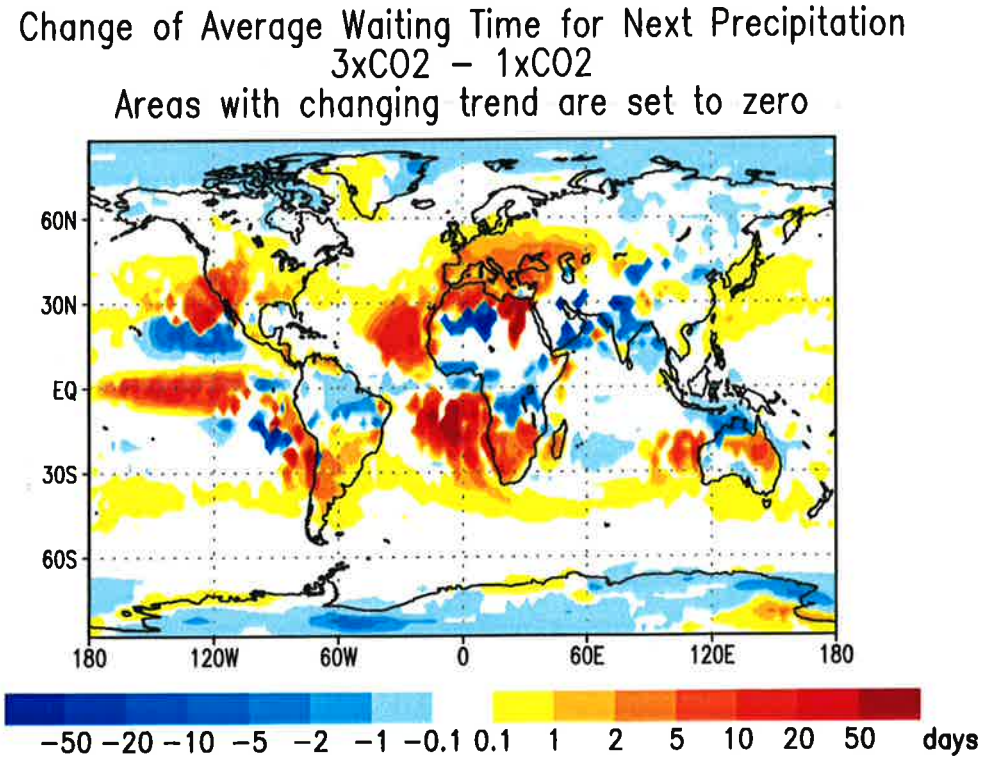

FIGURE 14. The regional distribution of the annual mean of the average waiting time for the next precipitation for the control integration (top) and its change in the 3*CO_2 integration relative to the control experiment (bottom). Regions, where the 2*CO_2 and 3*CO_2 simulation do not show the same trend or where the changes are not significant, have been blanked out.

The weaker forcing of the 2*CO_2 experiment does not allow the changes to emerge as clearly as in the 3*CO_2 experiment. A change in the seasonal cycle is frequently not yet visible in the 2*CO_2 experiment, but it becomes distinct in the 3*CO_2 experiment. The amplitude to the forcing is non-linear. The change for the 2*CO_2 experiment is only 30% to 40% of the change of the 3*CO_2 experiment.

A comparison with mixed-layer model results shows that the 3*CO_2 experiments resemble rather the results of the equilibrium 2*CO_2 experiments than the 2*CO_2 time-slice runs. As shown in (IPCC, 1990) the transient models have obtained at the time of CO_2 doubling only about 60% of the equilibrium warming, while by the time they have reached 3*CO_2, the transient experiment simulates about the equilibrium temperature change value.

Regional climate changes caused by different SST pattern distribution might have to be taken into consideration as well. As has been shown in Cubasch (1985) a tropical SST anomaly can cause significant changes in the vicinity of the anomaly, and can influence the flow pattern in the mid-latitudes in both hemispheres. However, this effect should not be of much importance, since the tropical SST taken in the tropical belt still correlates almost 80% between the two climate change simulations. The blurred picture of the climate change in Australia is caused by the combination of a tropical and a subtropical region. Here partially the opposite effects in the two different climate zones cancel each other out.

Nearly all continental regions with the exception of the higher latitudes have a negative correlation between the precipitation change and the temperature change, i. e. in those months when the temperature rise is largest, the precipitation change is minimal, and vice versa. This signal is particularly strong in the tropical regions of Africa and South America, and over India, Indonesia and Central and Southern Europe. Over North America this signal is not very distinct. In the polar regions, this correlation is reversed, i. e. in the months with the largest temperature increase also the precipitation increases.

The daily temperature contrast decreases over wide areas of the globe with the exception of Central and Southern Europe. Since this quantity has been measured regularly by meteorological services, it would be worthwhile to analyse it in more detail as has been done up to now, and to see, if the anomalous behavior over Europe can be found in observations as well. Furthermore, the change of the daily temperature contrast can in most regions be linked to a change in the cloud cover, a quantities archived in the meteorological services and easily observed from satellites.

Similarly the rain intensity and the average waiting time for rain can be used for the detection of climate change. Both are quantities, which have been regularly observed or can easily be derived from regularly observed parameters. Since both are regionally dependent, a comparison of the sign of the change could give an additional confidence into a possibly found climate change.

It has, however, to be stressed that these parameters and their changes are strongly dependent on the physical parameterization of the models and the realism of the simulated feedbacks. Most of these parameters have yet to be validated, and, considering the deviations in the simulation of the means of precipitation and temperature, they will certainly display large differences. The next generation of models with a higher resolution (T106 = Gaussian grid of ca. 1.1^{o}) simulates the climate more realistically (Arpe et al, 1994; Bengtsson et al, 1994), but still has appreciable problems with the hydrological cycle. A time slice integration has been done with this mode, but only for a period of five years and only for the $2*CO_2$ case. The higher resolution model shows a higher sensitivity to the radiative forcing, i. e. the seasonal cycle is altered already at $2*CO_2$. However, the small number of simulated years makes it impossible to assign any statistical significance to this result. A new model version (ECHAM4) overcomes some of the problems in the simulation of the temperature over North America (Roeckner, pers. com.) and generally is more realistic. It would be interesting to see if the parameter changes discussed here can be found in simulations of other modeling groups as well.

5.0 Acknowledgments

We would like to thank Arno Hellbach and Peter Lenzen for their support in the practical aspects of this work and K. Arpe, E. Roeckner, B. Machenhauer, H. von Storch as well as M. Lal and T. Karl for their helpful discussions. The research has been supported by the German Ministry for Research and Technology (BMFT), the Max-Planck-Gesellschaft, the Freie und Hansestadt Hamburg and the EC Environmental program. The authors are grateful to the staff of the DKRZ for their technical support.

6.0 References

Arpe, K., L. Bengtsson, L. Dümenil, and E. Roeckner, 1994: The hydrological cycle in the ECHAM3 simulations of the atmospheric circulation. in: *Global precipitation and climate change*, ed: Desbois M, Desalmond F, NATO ASI Series, Vol I, **26**, 361-377

Bengtsson, L., M. Botzet and M. Esch, 1994: Will greenhouse gas-induced warming over the next 50 years lead to higher frequency and greater intensity of hurricanes?. Report No. 139, Max-Planck-Institut für Meteorologie, Bundestr. 55, Hamburg, Germany.

Bengtsson, L., K. Arpe, E. Roeckner, and U. Schulzweida, 1994: Climate predictability experiments with a general circulation model. Report No. 145, Max-Planck-Institut für Meteorologie, Bundestr. 55, Hamburg, Germany.

Brinkop, S., 1991: Inclusion of cloud processes in the ECHAM PBL parameterization. Large Scale Atmospheric Modelling Rep. No. 9, 5-14, Met. Inst. Univ. Hamburg, Germany

Bücher, A. and J. Dessens, 1991: Secular trends of surface temperature at an elevated observatory in the Pyrenees. *J. Climate*, **4**, 859-868.

Cao, H. X., J. F. B. Mitchell amd J. R. Lavery, 1992: Simulated diurnal rage and variability of surface temperature in a global climate model for present and doubled CO_2 climates. *J. Climate*, **5**, 920-943.

Claussen, M., and M. Esch, 1992: BIOMES computed from simulated climatologies. Report No. 89, Max-Planck-Institut für Meteorologie, Bundestr. 55, Hamburg, Germany.

Cubasch, U., 1985: The mean response of the ECMWF global model to the El Nino anomaly in extended range prediction experiments; *Atmosphere-Ocean,* **23**, 43-66.

Cubasch, U., K. Hasselmann, H. Höck, E. Maier-Reimer, U. Mikolajewicz, B. D. Santer, and R. Sausen, 1992: Time-dependent greenhouse warming computations with a coupled ocean-atmosphere model. *Climate Dynamics,* **8**, 55-69

Cubasch, U., G. Hegerl, A. Hellbach, H. Höck, U. Mikolajewicz, B. D. Santer and R. Voss, 1994: A climate change simulation starting 1935. *Climate Dynamics,* in press.

DKRZ, 1993: The ECHAM3 atmospheric general circulation model. Techn. Rep. No. 6, DKRZ, Bundestr. 55, Hamburg, Germany

Dümenil, L., and E. Todini, 1992: A rainfall-runoff scheme for use in the Hamburg GCM. EGS Series on Hydrological Sciences, **1**, 129-157

Giorgi, F., and L. Mearns, 1991: Approaches to the simulation of regional climate change: A review. *J. Geophys. Res.,* **29**, 191-216

Gleckler, P. J., D. A. Randall, G. Boer, R. Colmann, M. Dix, V. Galin, M. Helfand, J. Kiehl, A. Kitoh, W. Lau, XZ Liang, V. Lykossov, B. McAvaney, K. Miyakoda, S. Planton, 1994: Cloud-radiative effects on implied oceanic energy transports as simulated

by atmospheric general circulation models. PCMDI Report No. 15, PCMDI/LLNL, Livermore, Ca., USA

Grotch, S. L., and M. C. McCracken, 1991: The use of general circulation models to predict regional climate change. *J. Climate,* **4**, 286-303

Hasselmann, K., R. Sausen, E. Maier-Reimer and R. Voss, 1992: On the cold start problem in transient simulations with coupled ocean-atmosphere models. Report No. 83, Max-Planck-Institut für Meteorologie, Bundestr. 55, Hamburg, Germany

Hense, A., M. Kerschgens and E. Raschke, 1982: An economical method for computing radiative transfer in circulation models. *Quart. J. Roy. Met. Soc.,* **108**, 231-252

IPCC, 1990: Climate change: The IPCC scientific assessment. Eds. J. Houghton, G. J. Jenkins and J. J. Ephraums, Cambridge University Press, 364 pp.

IPCC, 1992: Climate change: The supplementary report to the IPCC scientific assessment. Eds. J. Houghton, B. A. Callendar and S. K. Varney, Cambridge University Press, 198pp.

Karl,T.R., and R.W. Knight, 1994: Multi-decadal changes in precipitation frequency and intensity. 6th Symposium on Global Change Studies. Preprint Amer. Meteor. Soc.

Karl, T.R., Knight, R.W., N. Plummer, and V. Razuvayev, 1995: Temperature variability and precipitation extremes: Evidence for change. *In preparation.*

Lal, M., U. Cubasch, and B. D. Santer, 1994: Effect of global warming on Indian monsoon simulated with a coupled ocean-atmosphere general circulation model. *Current Science*, **66**, 430-438.

Legates, D. R., and C. J. Willmott, 1990: Mean seasonal and spatial variability in gauge corrected global surface air temperature. *J. Climatology,* **41**, 11-21

Legates, D. R., and C. J. Willmott, 1990: Mean seasonal and spatial variability in gauge corrected global precipitation. *J. Climatology,* **10**, 111-127

Lohmann, U., R. Sausen, L. Bengtsson, U. Cubasch, J. Perlwitz and E. Roeckner, 1993: The Köppen climate classification as a diagnostic tool for general circulation models. *Climate Research*, **3**, 177-193.

Louis, J. F., 1979: A parametric model of vertical eddy fluxes in the atmosphere. Boundary Layer Meteorology, **17**, 187-202.

Mahfouf, J. F., D. Cariolle, J.-F. Royer, J.-F. Geleyn, and B. Timbal, 1994: Responses of the Meteo-France climate model to changes in CO_2 and sea surface temperature. *Climate Dynamics*, **9**, 345-362.

Miller, M. J., T. N. Palmer, and R. Swinbank, 1989: Parameterization and influence of sub-grid scale orography in general circulation and numerical weather prediction models. *Met. Atm. Phys.,* **40**, 84-109.

Parey, S., 1994 : $2xCO_2$ and $3xCO_2$ time slice experiments. Change in mean and variability - 19th General Assembly of the European Geophysical Society - Grenoble,

Perlwitz, J., U. Cubasch, and E. Roeckner, 1994: Simulation of greenhouse warming with the ECHAM3 model using the time-slice method. Report, Max-Planck-Institut für Meteorologie, Bundestr. 55, Hamburg, Germany, *in preparation*.

Roeckner, E., K. Arpe, L. Bengtsson, S Brinkop, L. Dümenil, M. Esch, E. Kirk, F. Lunkeit, M. Ponater, B. Rockel, R. Sausen, U. Schlese, S. Schubert, and M. Windelband, 1992: Simulation of the present-day climate with the ECHAM model: impact of model physics and resolution. Report No. 93, Max-Planck-Institut für Meteorologie, Bundestr. 55, Hamburg, Germany.

Rockel, B., E. Raschke, and B. Weynes, 1991: A parameterization of broad band radiative transfer properties of water, ice and mixed clouds. *Beitr. Phys. Atmos.*, **64**, 1-12.

Santer, B. D., U. Cubasch, U. Mikolajewicz,and G. Hegerl, 1993: The use of general circulation models in detection climate change induced by greenhouse gases. PCMDI Report No. 10, PCMDI/LLNL, Livermore, Ca., USA

Santer B. D. , W. Brüggemann, U. Cubasch, K. Hasselmann, E. Maier-Reimer und U. Mikolajewicz, 1994: Signal-to-noise analysis of time-dependent greenhouse warming experiments. Part 1: Pattern analysis. *Climate Dynamics*, **9**, 267-285.

Tiedtke, M., 1989: A comprehensive mass flux scheme for cumulus parameterization in large-scale models. *Mon. Wea. Rev.*, **117**, 1779-1800

von Storch, H., E. Zorita, and U. Cubasch, 1993: Downscaling of global climate change estimates to regional scales: an application to Iberian rainfall in wintertime. *Journal of Climate,* **6**, 1161-1171.

Whetton, P. H., A. M. Fowler, M. R. Haylock, and A. B. Pittock, 1993: Implications of climate change due to the enhanced greenhouse effect on floods and droughts in Australia. *Climate Change,* **25**, 289-317.

Wigley, T. M. L., P. D. Jones, K. R. Briffa, and G. Smith, 1990: Obtaining subgrid scale information from coarse-resolution general circulation model output. *J. Geophys. Res.*, **95**, 1943-1953.